An Analysis and Classification of Dying AGB Stars Transitioning to Pre-Planetary Nebulae

Adam C. Blake

JET PROPULSION LAB

Major: Engineering Physics

USRP Spring Session

Date: 02 MAY 11

An Analysis and Classification of Dying AGB Stars Transitioning to Pre-Planetary Nebulae

Adam Blake[1] and Raghvendra Sahai[2]
NASA Jet Propulsion Laboratory, Pasadena, CA, 91109

Abstract

The principal objective of the project is to understand part of the life and death process of a star. During the end of a star's life, it expels its mass at a very rapid rate. We want to understand how these Asymptotic Giant Branch (AGB) stars begin forming asymmetric structures as they start evolving towards the planetary nebula phase and why planetary nebulae show a very large variety of non-round geometrical shapes. To do this, we analyzed images of just-forming pre-planetary nebula from Hubble surveys. These images were run through various image correction processes like saturation correction and cosmic ray removal using in-house software to bring out the circumstellar structure. We classified the visible structure based on qualitative data such as lobe, waist, halo, and other structures. Radial and azimuthal intensity cuts were extracted from the images to quantitatively examine the circumstellar structure and measure departures from the smooth spherical outflow expected during most of the AGB mass-loss phase. By understanding the asymmetrical structure, we hope to understand the mechanisms that drive this stellar evolution.

This research was carried out at the Jet Propulsion Laboratory, California Institute of Technology and was sponsored by the Undergraduate Student Research Program (USRP) and the National Aeronautical and Space Administration.

I. Background

The purpose of this document is to summarize all activities and processes done in my spring internship at the Jet Propulsion Lab (JPL) in Pasadena, California. The mentor for my project was Raghvendra Sahai. This project builds on the work of a previous intern, Charlotte Blumenfeld.

When sun-like stars get old, they become cooler and redder, increasing their sizes and energy output tremendously; they are called red giants. When they are at the very end of the evolutionary phase and known as Asymptotic Giant Branch (AGB) stars, they have sizes of a few AU, luminosities 10,000 times that of the Sun, and effective temperatures of 2500-3000K. Most of the carbon (the basis of life) and particulate matter (crucial building blocks of solar systems like ours) in the universe is manufactured and dispersed by red giant stars. The stars are surrounded by a large (sizes $>\sim$ few x 10^4 AU), spherical, slowly expanding (with speeds of ~10-20 km/s) circumstellar envelope composed of molecular gas and dust which have been ejected by the star. Planetary nebulae (PNe) are formed when these stars have ejected all of their outer layers, exposing its very hot core (six or more times hotter than the Sun). Nascent pre-planetary nebulae, the objects being studied here, represent the earliest phase of the transformation of AGB stars to PNe.

II. Sources

The sources of interest are listed in Table 1. The proposal ID is the original proposal for which the source was imaged. The detectors are part of the Hubble Space Telescope's (HST) Advanced Camera for Surveys (ACS). The

[1] USRP Intern, Astrophysics and Space Science, JPL, Embry-Riddle Aeronautical University.
[2] Principal Research Scientist, Astrophysics and Space Science, 183-900, JPL.

ACS has three channels, the High-Resolution channel (HRC), the Wide Field channel (WFC), and the Solar Blind Channel (SBC) (Wikipedia, 2011). In the HRC, 1 pixel is equivalent to 0.025 arc seconds. In the WFC, 1 pixel is equivalent to 0.050 arc seconds. The image orientation refers to the position angle of the y-axis of the image. The angle is measured counterclockwise from north to east.

Table 1. Source Data

Name of Source	Proposal ID	Date of Observation	Detector	Image Orientation (deg)
IRAS00247+6922	10185	8/17/2004	WFC	-141.6613489
IRAS02316+6455	10185	9/25/2004	HRC	-0.000476868
IRAS03507+1115	10185	8/12/2004	HRC	76.51428082
IRAS05411+6957	10185	12/1/2004	HRC	-0.000139033
IRAS06300+6058	10185	12/1/2004	HRC	-0.000446599
IRAS06500+0829	10185	12/11/2004	HRC	0.000639479
IRAS07454-7112	10185	9/12/2004	HRC	54.66592433
IRAS08088-3243	10185	2/1/2005	HRC	-5.80431E-05
IRAS09521-7508	10185	2/2/2005	HRC	0.000472271
IRAS12540-6845	10185	12/27/2004	HRC	0.00009.67268
IRAS13421-6125	9463	3/20/2003	HRC	150.1003144
IRAS13442-6109	10185	8/8/2004	HRC	-63.83400943
IRAS14562-5406	9463	3/9/2003	HRC	121.7417352
IRAS15082-4808	10185	8/11/2004	HRC	-77.14835287
IRAS15099-5509	10185	1/20/2005	WFC	-0.020773535
IRAS15194-5115	10185	8/11/2004	HRC	-79.80850915
IRAS16006-5257	10185	5/13/2005	HRC	161.4515038
IRAS16122-5128	10185	7/1/2005	HRC	-118.7994273
IRAS16545-4214	10185	1/28/2005	HRC	-0.000305613
IRAS17163-3907	10185	8/31/2004	HRC	-89.63251838
IRAS17187-3750	10185	3/10/2005	HRC	-9.80299E-05
IRAS17297+1747	10185	5/17/2005	HRC	38.91357027
IRAS17319-6234	10185	3/13/2005	HRC	-0.000126141
IRAS17360-3012	9463	3/7/2003	WFC	-88.96126614
IRAS17446-7809	10185	10/13/2004	HRC	0.000314801
IRAS18009-2019	10185	4/30/2005	HRC	87.0022565
IRAS18204-1344	10185	3/7/2005	HRC	90.98649066
IRAS18267-0606	10185	5/16/2005	HRC	68.99714879
IRAS18349+1023	10185	3/28/2005	HRC	87.22848962
IRAS18387-0423	10185	5/29/2005	HRC	58.92780157
IRAS18397+1738	10185	11/7/2004	HRC	-0.000381338
IRAS18398-0220	10185	4/19/2005	HRC	79.06943026
IRAS18467-4802	10185	3/13/2005	WFC	-0.015130997
IRAS18560-2954	10185	4/30/2005	HRC	87.68006053
IRAS18595-3947	10185	3/12/2005	HRC	-0.000362831
IRAS19008+0726	10185	11/6/2004	HRC	-0.000327039
IRAS19059-2219	10185	3/11/2005	HRC	-0.000279413
IRAS19126-0708	10185	10/12/2004	HRC	-0.000290814
IRAS19135+0931	10185	6/20/2005	HRC	29.47328371
IRAS19321+2757	10185	9/28/2004	HRC	-83.44994049
IRAS19474-0744	10185	3/15/2005	HRC	87.6821725
IRAS20077-0625	10185	9/14/2004	WFC	88.91579975
IRAS20310+4029	10185	9/29/2004	HRC	0.000202144

Name of Source	Proposal ID	Date of Observation	Detector	Image Orientation (deg)
IRAS20312+4035	10185	11/14/2004	HRC	-0.000312142
IRAS20396+4757	10185	10/25/2004	HRC	-0.0000287701
IRAS23320+4316	10185	2/7/2005	HRC	-145.3802701
IRAS23496+6131	10185	8/9/2004	HRC	37.34565139

III. Image Processing

All images processed for this paper are from the MAST database. MAST stands for the Multimission Archive at STScI (Space Telescope Science Institute). All images were downloaded from this public database and were processed mainly with JPL in-house software known as SPICA (Shell for Processing Images with Coordinated Algorithms). Image processing included removing image saturation, measuring image offset, and shifting images. Intensity cuts were then taken of the images, in both the radial and azimuthal directions. This gave quantitative data to define nebula structure.

Each source had anywhere from four to eight images. Each source was imaged in two filters using either the 435 nm, 606 nm or 814 nm filters. Examples for some of these sources are below.

IRAS 19008+0726

File Name	Filter	Exposure Time
J92k44011	606	250 sec
J92k44021	606	60 sec
J92k44031	606	5 sec
J92k44041	814	50 sec
J92k44051	814	12 sec
J92k44061	814	2 sec
J92k44071	814	50 sec
J92k44081	606	250 sec

IRAS 00247+6922

File Name	Filter	Exposure Time
J92k01fsq	606	347 sec
J92k01ftq	814	347 sec
J92k01fvq	814	347 sec
J92k01fxq	606	347 sec

Operational details of the scripts used to carry out steps 1-4 (below) are described in the Appendix.

Step 1 – Offset Measurment

The first processing step was to measure the offset between a pair of equal-exposure, dithered images. By combining two dithered images, one can improve resolution when the pixel size is comparable to the intrinsic resolution of the telescope, causing inadequate sampling of the point-spread function (PSF).

Step 2 - Saturation

After measuring the offset, the next step is to check for saturation and bleeding. A Charged-Couple Device (CCD) works by converting light (photons) into charge (electrons) which are stored in the pixel's potential well. When the pixel's well gets filled to capacity, the pixel is considered saturated. Sometime a pixel becomes so saturated with charge that the charge will spill onto adjacent pixels. This is known as bleeding.

The script for checking for saturation involves a long and short exposure image. Each of the images should have the same linear ratio of CCD charge to image exposure. As exposure time increases, the potential well will fill up and this ratio changes. Saturation and bleeding can be seen in Fig. 1. If saturation is found, another script is run to correct it. In the script, the sound to noise ratio for pixels is computed and saturated pixels are replaced with appropriate values. If there is a medium exposure image available, it is used in the saturation correction process. The short exposure image is used to fix any saturation in the medium exposure image. Then, the corrected medium exposure image is used to fix the saturation in the long exposure image. Using the medium exposure image, it

allowed for saturated pixels further from the source to be corrected. Each time the script is run, it outputs the corrected image. This corrected image can be plotted exactly the same as earlier when checking for saturation (which has been done in Fig. 2). By simply comparing the images, the saturation is removed.

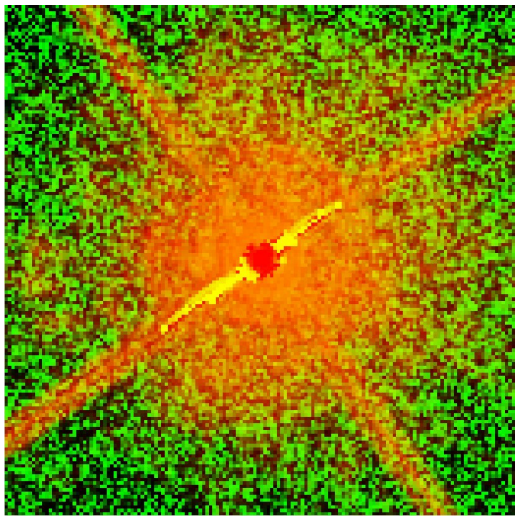

Figure 1. Saturated Image IRAS 06500 606 Filter (3.75 arcsec x 3.75 arcsec)

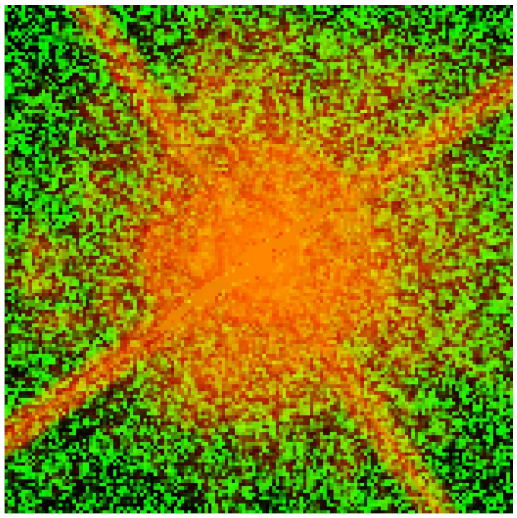

Figure 2. Unsaturated Image IRAS 06500 606 Filter (3.75 arcsec x 3.75 arcsec)

Step 3 – Shifting Images

The dithered images are shifted using the offsets found in the first step. Once the shifts were done, they need to be checked, just like saturation was checked after fixing it. To check image shifts, all four images (the three shifted images and the one they were shifted relative to) are read into SPICA. SPICA is used to subtract one image from another and display them as shown in Fig. 3 & 4. To determine if a shift is good, the displayed image should not have a distinctive black and white half. In Fig.3, the background stars have no black and white half. However, in Fig.4, there are black and white halves in the background stars. The background stars are white on the left and black on the right. However, for Fig. 3, the background stars are black in the middle and white around the edges. If a shift is bad, as in Fig. 4, the offset values will need to be changed and images reshifted in IRAF.

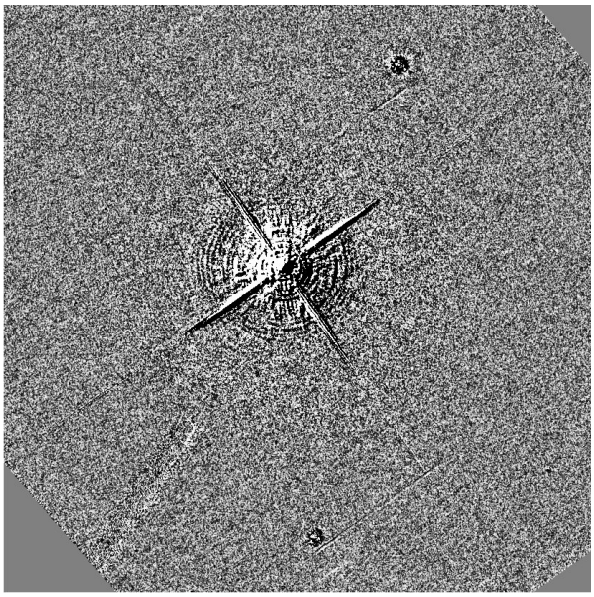

Figure 3. Good Shift IRAS 06500 606 Filter (21.25 arcsec x 21.25 arcsec)

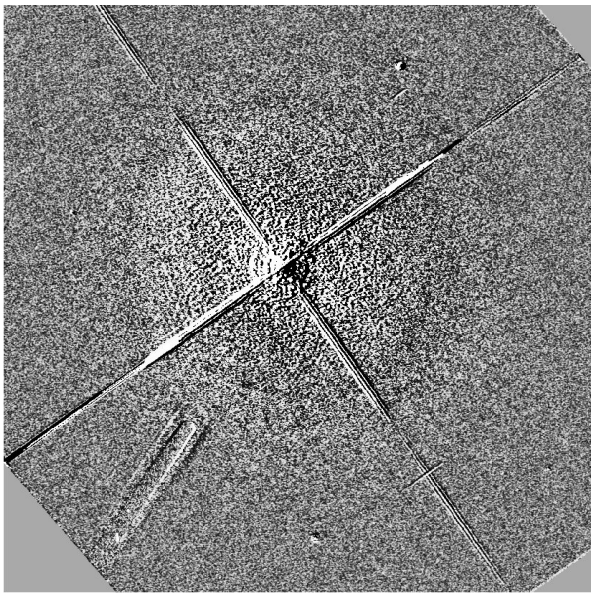

Figure 4. Bad Shift IRAS 06500 606 Filter (21.25 arcsec x 21.25 arcsec)

Step 4 – Cosmic Ray Removal and Averaging

The next step is to remove cosmic rays from the images and average the long exposure images. This is done for each filter using its two long exposure images that have been processed through the previous steps. The script computes the signal noise per pixel based on the exposure time. If a pixel vastly exceeds the average pixel noise, it is replaced by that average. This produces the final calibrated science image.

IV. Analysis of Circumstellar Structure

The importance of characterizing the circumstellar structure is to understand the mass-loss process. The mass-loss process of the stars that form planetary nebulae, i.e. AGB stars, is thought to produce a slowly expanding (~10-20 km/s) wind, and thus a smooth, round circumstellar envelope. However, the presence of asymmetric circumstellar structures suggests departures from this expectation and suggests additional physical mechanisms at work. Some of these asymmetric structures include arc structures (Fig. 5&6), elongation (Fig. 7), collimation (Fig. 8) and an irregular (non-circular) center. Sahai & Trauger (1998) proposed that collimated fast wind or jets (CFW) were responsible for the shaping of planetary nebula [2]. The finding of elongated structures in a small fraction of the observed sample suggests that we are observing the earliest stages of operation of the CFW's (Sahai, 2007). These structures are created when the CFW interacts with the spherical radiative wind from the star, shaping the circumstellar structure before the planetary nebula stage. By studying the elongated and collimated structures, we can study the CFWs. However, the CFWs are most likely not responsible for the arc-like structures. Further investigation of these arc structures should help us learn the mechanism that forms them.

A. Sharpening Scripts

Any of the images can then be run through a sharpening and smoothing script. The purpose of this script is to bring out any defined edges and to smooth out the background so these edges can be better seen. Fig. 5 & 6 are the sharpened images for source IRAS 08088-3243. The sharpening has brought out a few arcs in the lower left. They are on either side of the background star. The images also show that the center is irregular, not circular.

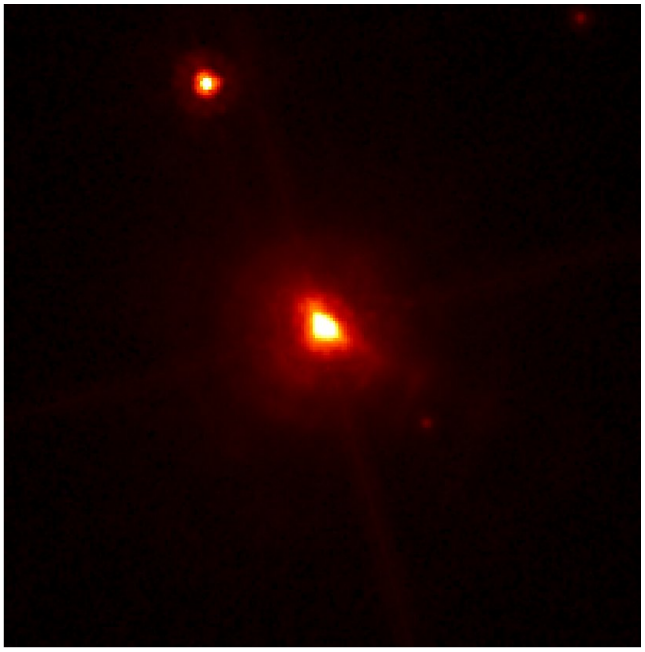

Figure 5. IRAS 08088 606 Filter (5.525 arcsec x 5.575 arcsec)

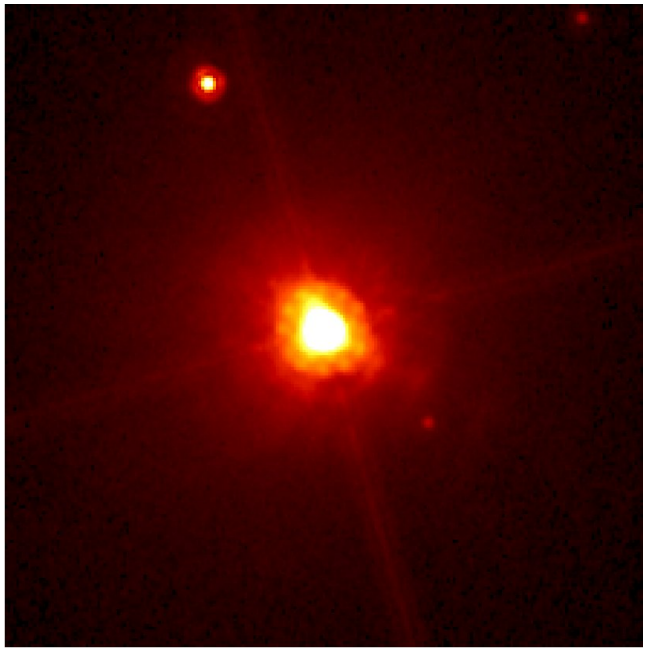

Figure 6. IRAS 08088 814 Filter (5.525 arcsec x 5.575 arcsec)

The images of each source were processed through steps 1-4 and the characteristics of the circumstellar structure were recorded in Table 2.

Table 2. Structure Characteristics

Name of Source	Filter	CSE[3]	PSF[4]	DS[5]	CC[6]	Description of Circumstellar Structure
IRAS00247+6922	606W	no	yes	yes	no	Irregular
	814W	no	yes	yes	no	Irregular
IRAS02316+6455	606W	no	no	no	no	Regular
	814W	no	yes	yes	no	Regular
IRAS03507+1115	435W	yes	no	no	no	Regular
	606W	yes	yes	yes	no	Elongated
IRAS05411+6957	435W	no	no	no	no	Regular
	606W	no	yes	yes	no	Irregular
IRAS06300+6058	606W	yes	yes	yes	no	Irregular
	814W	yes	yes	yes	no	Irregular
IRAS06500+0829	606W	yes	yes	yes	no	Arc Structure
	814W	yes	yes	yes	no	Arc Structure
IRAS07454-7112	606W	yes	yes	yes	no	Elongated
	814W	yes	yes	yes	no	Elongated
IRAS08088-3243	606W	yes	yes	yes	no	Arc Structure, Elongated, Irregular
	814W	yes	yes	yes	no	Arc Structure, Elongated, Irregular
IRAS09521-7508	606W	no	yes	yes	no	Irregular
	814W	no	yes	yes	no	Irregular
IRAS10323-4611	606W	yes	no	no	yes	Elongation
	814W	yes	yes	yes	yes	Elongation, Possible Arcs
IRAS12540-6845	606W	yes	yes	yes	No	Irregular
	814W	yes	yes	yes	no	Regular
IRAS13421-6125	606W	yes	yes	yes	no	Regular
	814W	yes	yes	yes	no	Regular
IRAS13442-6109	606W	no	yes	yes	no	Elongated
	814W	no	yes	yes	no	Elongated
IRAS15082-4808	606W	yes	no	no	no	Elongated with Irregularities
	814W	yes	no	no	no	Elongated with Irregularities
IRAS15099-5509	606W	yes	no	no	yes	Elongation
	814W	?	yes	yes	yes	Obscured by Saturation
IRAS15194-5115	606W	no	yes	yes	no	Regular
	814W	no	yes	yes	no	Regular
IRAS16006-5257	606W	no	yes	no	no	Regular
	814W	no	yes	yes	no	Regular
IRAS16122-5128	606W	no	yes	yes	yes	Irregular, Possible Lobes
	814W	no	yes	yes	yes	Irregular, Possible Lobes
IRAS16545-4214	606W	no	no	yes	yes	Irregular, Collimated
	814W	no	no	yes	yes	Irregular, Collimated
IRAS17163-3907	435W	no	yes	yes	no	Irregular
	606W	no	yes	yes	no	Irregular
IRAS17187-3750	606W	no	yes	yes	yes	Irregular
	814W	no	yes	yes	yes	Irregular
IRAS17297+1747	606W	no	yes	yes	no	Regular

[3] CSE: Circumstellar Envelope
[4] PSF: Point Spread Function
[5] DS: Diffraction Spikes
[6] CC: Close Companion

Name of Source	Filter	CSE[3]	PSF[4]	DS[5]	CC[6]	Description of Circumstellar Structure
	814W	no	yes	yes	yes	Regular
IRAS17319-6234	606W	no	yes	yes	no	Regular
	814W	no	yes	no	no	Regular
IRAS17360-3012	606W	no	yes	no	no	Regular
	814W	no	yes	no	no	Regular
IRAS17446-7809	606W	yes	yes	yes	no	Elongated
	814W	yes	yes	yes	no	Regular
IRAS18009-2019	606W	no	yes	yes	no	Regular
	814W	no	yes	yes	no	Arc Structure
IRAS18204-1344	435W	no	yes	yes	no	Irregular
	606W	no	yes	yes	no	Irregular
IRAS18267-0606	606W	no	yes	yes	no	Irregular
	814W	no	yes	yes	no	Irregular
IRAS18349+1023	606W	no	yes	yes	no	Regular
	814W	no	yes	yes	no	Regular
IRAS18387-0423	435W	no	yes	yes	no	Regular
	606W	no	yes	yes	no	Regular
IRAS18397+1738	606W	yes	yes	yes	yes	Partial Round Arc, Collimated
	814W	yes	yes	yes	yes	Partial Round Arc, Collimated
IRAS18398-0220	606W	no	yes	yes	no	Regular
	814W	no	yes	yes	no	Regular
IRAS18467-4802	606W	Source Obscured In Image				
	814W	yes	no	no	no	Regular
IRAS18560-2954	606W	yes	no	no	no	Elongated with irregularities
	814W	yes	no	no	no	Elongated with irregularities
IRAS18595-3947	606W	yes	yes	yes	no	Collimated
	814W	yes	yes	yes	no	Collimated
IRAS19008+0726	606W	yes	no	yes	no	Irregular, Collimated
	814W	yes	no	yes	no	Irregular, Collimated
IRAS19059-2219	606W	no	yes	yes	no	Regular
	814W	no	yes	yes	no	Regular
IRAS19126-0708	435W	no	yes	yes	yes	Irregular
	606W	no	yes	yes	yes	Irregular
IRAS19135+0931	606W	no	yes	no	no	Elongated
	814W	no	yes	yes	no	Elongated
IRAS19321+2757	606W	no	yes	yes	no	Elongated
	814W	no	yes	yes	no	Elongated
IRAS19474-0744	435W	no	yes	yes	no	Irregular
	606W	no	yes	yes	no	Irregular
IRAS20077-0625	606W	yes	no	no	no	Elongated
	814W	yes	no	no	no	Elongated, Collimated
IRAS20310+4029	435W	no	no	no	no	Elongated
	606W	no	yes	yes	yes	Elongated
IRAS20312+4035	606W	no	yes	yes	no	Regular
	814W	no	yes	yes	no	Regular
IRAS20396+4757	606W	no	yes	yes	no	Elongated
	814W	no	yes	yes	no	Elongated
IRAS23320+4316	606W	yes	no	no	no	Elongated, Collimated
	814W	yes	yes	yes	no	Elongated, Collimated

Name of Source	Filter	CSE[3]	PSF[4]	DS[5]	CC[6]	Description of Circumstellar Structure
IRAS23496+6131	606W	no	yes	no	no	Regular
	814W	no	yes	yes	no	Regular

B. Intensity Cuts

Intensity cuts, both radial and azimuthal, were taken of sources that show arc structures, elongation, and collimation. This allows us to characterize these features quantitatively. Fig. 8-10 are intensity cuts of the image shown in Fig. 7. The angle is measured counter-clockwise from the horizontal axis.

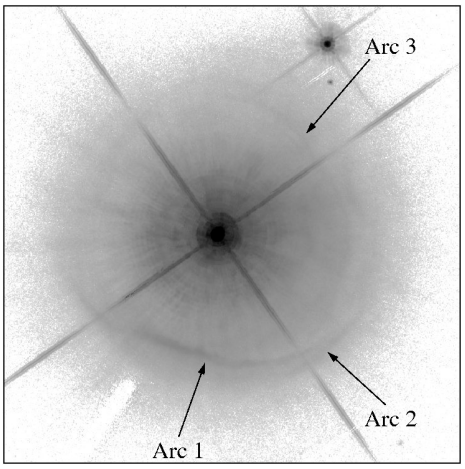

Figure 7. IRAS06500 606 Filter (17.525 arcsec x17.525 arcsec)

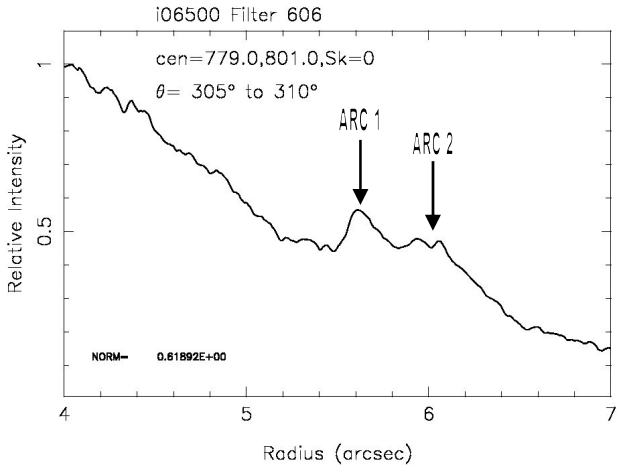

Figure 8. Intensity Cut 305° to 310°

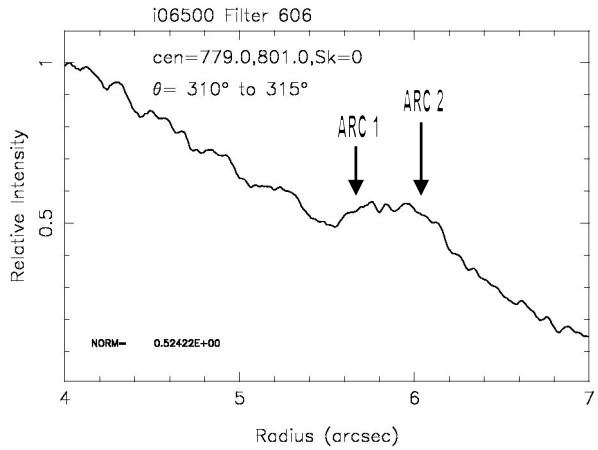

Figure 9. Intensity Cut 310° to 315°

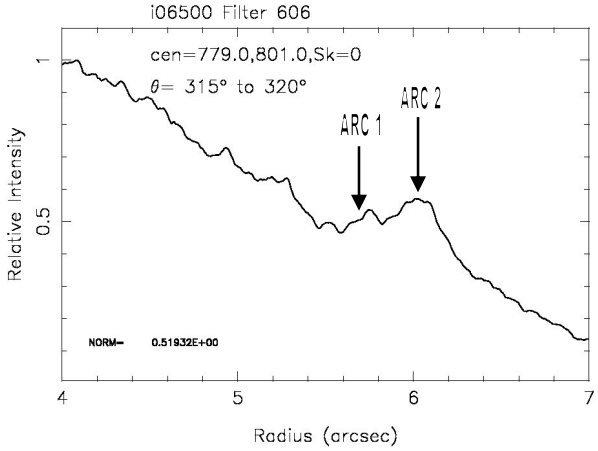

Figure 10. Intensity Cut 315° to 320°

These intensity cuts show a transition from Arc 1 to Arc 2. Using the intensity cuts, we can quantitatively characterize the circumstellar structure for this source. These sources as well as other sources are in Table 3.

Table 3. Radial Intensity Cuts

Source	Feature Name	Azimuthal Angle Range	Radius Range (arcsec)	Contrast
IRAS 06500	Arc1	200 deg. – 45 deg.	4.55 – 5.72	2.0
	Arc2	295 deg. – 335 deg.	5.83 – 6.10	1.4
	Arc3	45 deg. – 90 deg.	4.85 – 5.22	1.2
IRAS 08088	Arc1	305 deg. – 345 deg.	0.953 -1.007	2.05
	Arc2	315 deg. – 360 deg.	1.550 – 1.600	1.51
	Arc3	150 deg. – 205 deg.	1.277 – 1.316	1.40
IRAS 10323	Arc1	260 deg. – 330 deg.	1.121 – 1.207	2.27
IRAS 13442	Arc1	25 deg. – 100 deg.	0.754 – 0.855	2.19
	Arc2	250 deg. – 280 deg.	0.679 – 0.784	2.02
	Arc3	115 deg. – 145 deg.	0.587 – 0.642	1.88
IRAS 15082	Arc1	295 deg. – 325 deg.	0.683 – 0.736	1.36
IRAS 18009	Arc1	20 deg. – 70 deg.	0.471 – 0.593	1.63
	Arc2	335 deg. – 40 deg.	0.641 – 0.815	1.30
	Arc3	200 deg. – 260 deg.	0.637 – 0.703	1.22

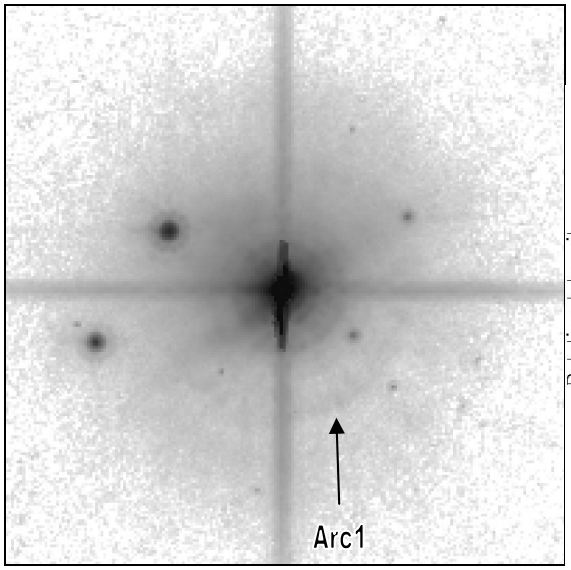

Figure 11. IRAS 10323 814 Filter (5.0 arcsec x 5.0 arcsec)

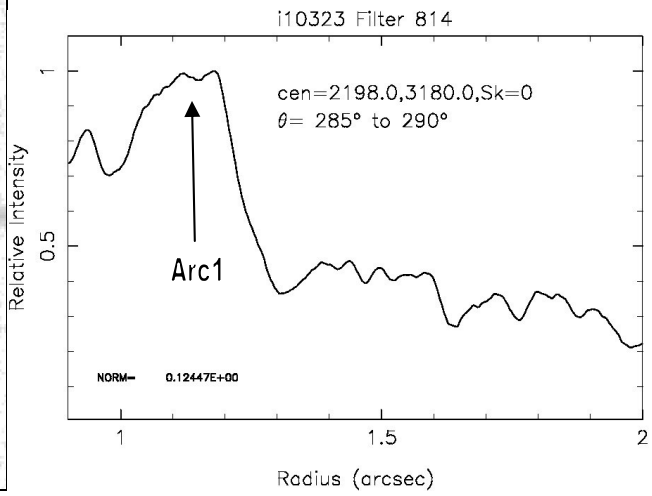

Figure 12. Intensity Cut 285° to 290°

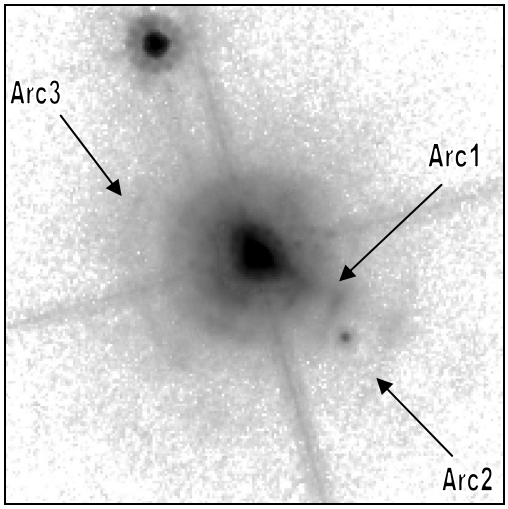

Figure 13. IRAS 08088 606 Filter (9.375 arcsec x 10.0 arcsec)

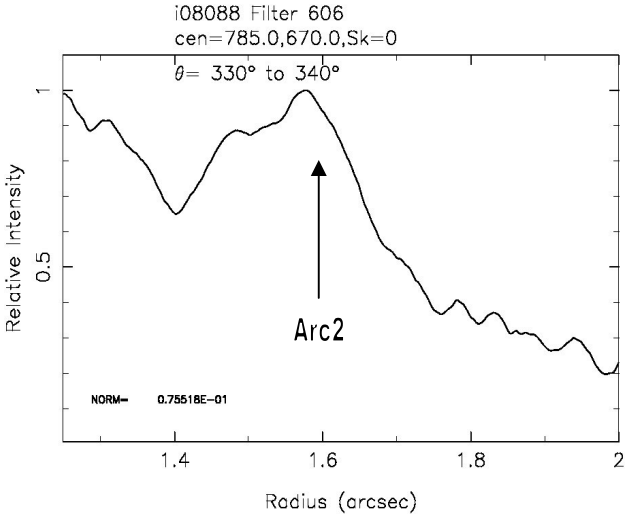

Figure 14. Intensity Cut 330° to 340°

As radial cuts were taken to analyze the arc structure, azimuthal intensity cuts taken to help analyze the elongated and collimated features. One hindrance with azimuthal intensity cuts it they also include the diffraction spikes present in some images. The diffraction spikes can be distinguished from radial structures in some sources, however, in other source (like IRAS 20077-0625), diffraction spikes inhibit complete circumstellar analysis due to overlap. For IRAS 23320+4316, the intensity cuts show that the opening angle (FWHM of the feature) becomes smaller at large radii, confirming the highly collimated nature of this feature. Additional results are shown in Table 4.

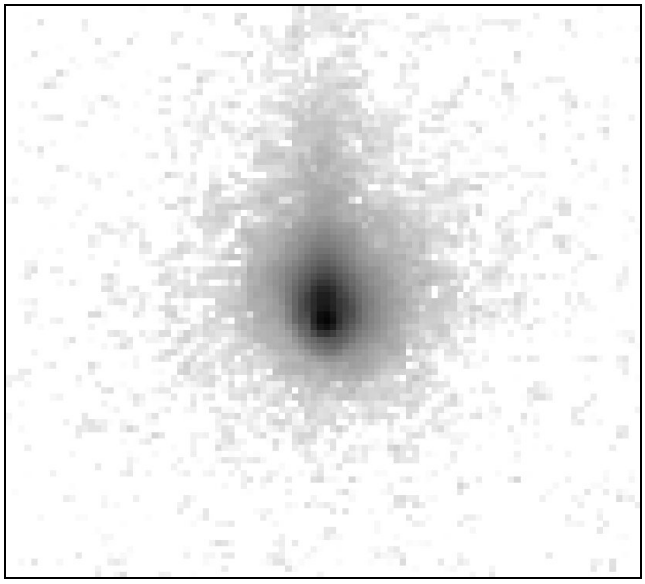

Figure 15. IRAS 23320 606 Filter (2.5 arcsec x 2.5 arcsec)

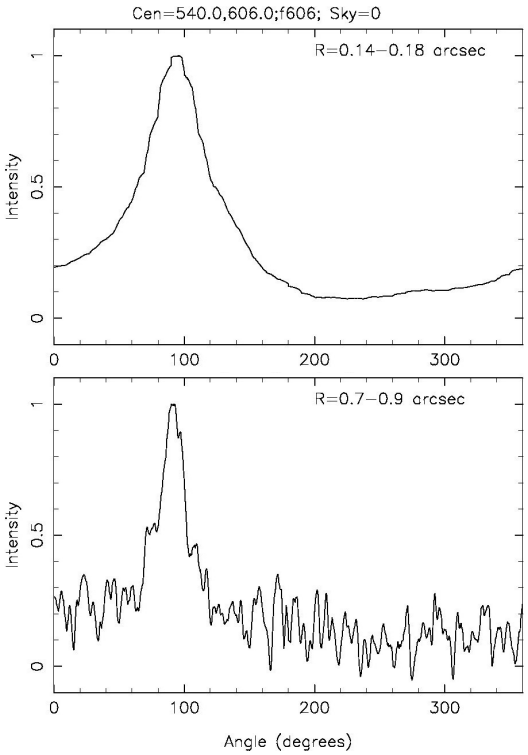

Figure 16. Intensity Cuts for IRAS 23320

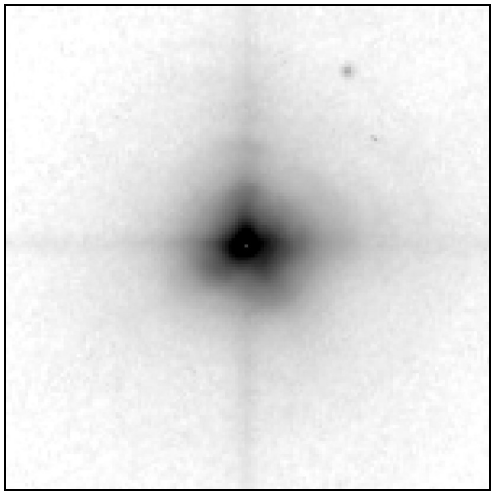

Figure 17. Source IRAS 20077 (7.5 arcsec x 7.5 arcsec)

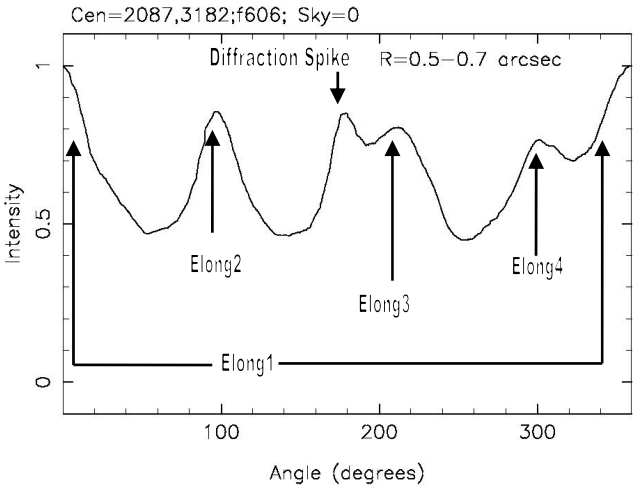

Figure 18. Intensity Cut for IRAS 20077

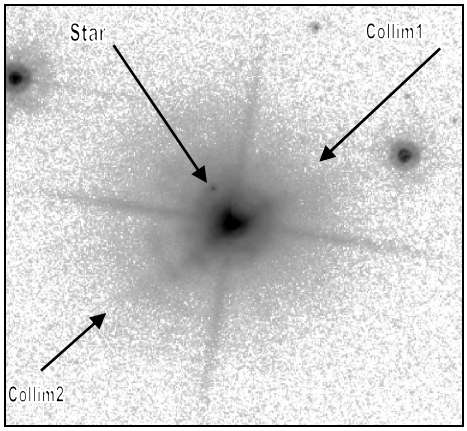

Figure 19. Source IRAS 16545 (9.525 arcsec x 8.775 arcsec)

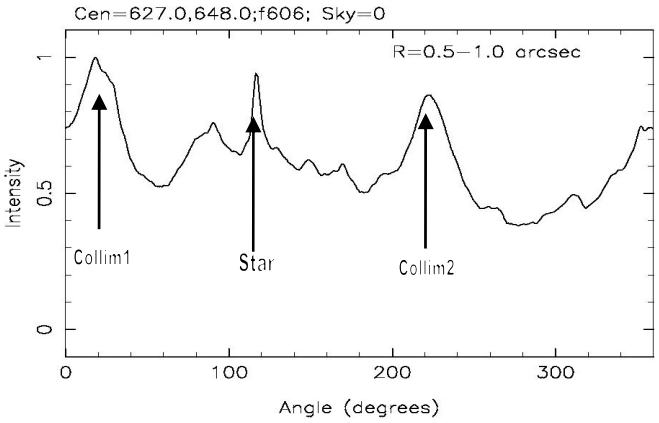

Figure 20. Intensity Cut for IRAS 16545

Table 4. Azimuthal Intensity Cuts

Source	Feature Name	Azimuthal Angle Range	Maximum Radial Distance
IRAS 23320	Elong 1	60 deg. – 140 deg.	1.7 arc seconds
IRAS 20077	Elong 1	-20 deg. – 30 deg.	Diffraction Spikes Interfere
	Elong 2	65 deg. – 125 deg.	Diffraction Spikes Interfere
	Elong 3	260 deg. – 240 deg.	1.5 arc seconds
	Elong 4	250 deg. – 325 deg.	1.5 arc seconds
IRAS 16545	Col 1	0 deg. – 40 deg.	2.9 arc seconds
	Col 2	200 deg. – 240 deg.	2.7 arc seconds

V. Conclusions & Future Work

This work shows that we can classify the circumstellar structure of nascent pre-planetary nebulae. We find a variety of asymmetrical structure such as arcs and radially collimated features - in these cases, we have measured the angular extents of the arcs and the opening angles of collimated features. For some sources, the central sources have a non-round, irregular shape. However, the classification work is not complete. Further work includes finishing intensity cuts for all interesting sources and cataloging their circumstellar structure, which includes measuring the degree of collimation of all radially-elongated features as a probe of the jet-like outflows proposed to explain such features. In addition, all point spread functions need to be removed. Over 80% of images contained point spread functions. Removing these would allow for better analysis of structure. We also need to look for correlations between the circumstellar structures that we have found and other properties of our sources such as circumstellar expansion velocities and mass-loss rates.

Appendix

- Measuring Offsets

The script for measuring the dithered distance first displays two selected images in two different color planes in SPICA. The first step is selecting the red color plane and using the cursor to mark the center of the stars, as many as possible. Once this is done, I switched to the blue color plane and the same stars were marked. The program then takes these points and computes the difference in pixels and finds the average offset and the rms error. For Fig. 21, I used the 606 filter images and used 4 stars in the background. It produced the following offset results.

X offsets -3.04779 -3.04468 -3.02563 -3.04102
Y offsets 1.47739 1.46939 1.49719 1.45801
X offsets, RMS and MEAN 0.00982803 -3.03978
Y offsets, RMS and MEAN 0.0165067 1.47549

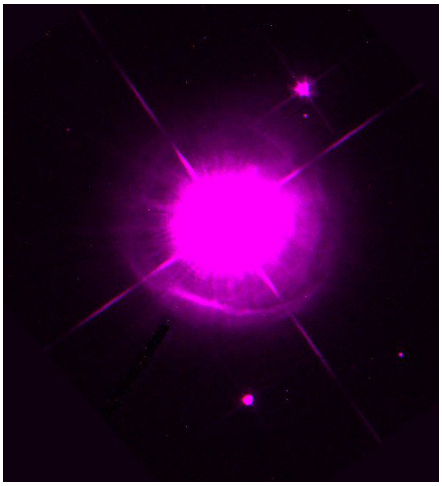

Figure 21. Offset Image

- Saturation

The script first plots the long exposure image in red. It then plots the ratio of the long to short exposure image in green. By plotting it in two different colors, those that combine to the color yellow show the saturation. An example is in Fig. 1. The red part in the middle is where the saturation is and the yellow streaks are the bleeding from the saturated center.

- Shifting Images

Instead of using SPICA for this step, IRAF (Image Reduction and Analysis Facility) was used. IRAF is a collection of software used by the National Optical Astronomy Observatory. IRAF's imshift command was used to shift the images and it reads in three text files. The first file contains the names of the images to be shifted; the images and file must be in the same directory. The second file is the name under which the shifted images are to be saved. The third file contains the shifting numbers found in the first step. The images being shifted are three of the four long exposures. An example of these files and the IRAF command is as follows:

File 1- fits.inp	File 2 – fits.out	File 3 – shifts
31_usat.fits	sh31.fits	-0.0001 -0.4823
61_usat.fits	sh61.fits	-2.8060 -2.1827
81_usat.fits	sh81.fits	-2.8806 -1.6360

imshift @fits.inp @fits.out shifts_file=shifts

When redoing bad shifts, it is best to correct one direction at a time, meaning change either the x or y value each time, not both.

- Logarithmic Scale

During image processing steps, an image can be displayed in a logarithmic scale. This way, a larger dynamical range can be seen in the image. It is a short ten line script that just reads in the image, converts the linear scale to a logarithmic scale, displays the image and saves it.

References

[1] "Advanced Camera for Survey," *Wikipedia* [Online Encyclopedia], Latest Revision: 4th February 2011, URL: http://en.wikipedia.org/wiki/Advanced_Camera_for_Surveys [cited 29th April 2011]

[2] Sahai, R., & Trauger, J.T. 1998, AJ, 116, 1357

[3] Sahai, R. 2007, "From AGB Stars to Planetary Nebulae -- How the Journey Begins", in Asymmetric Planetary Nebulae IV, proc. conference held in La Palma, Spain, June 2007, eds. R.L.M. Corradi, A. Manchado & N. Soker (in press)